THESIS FOR THE DEGREE OF LICENTIATE OF ENGINEERING

Waveguide Quantum Electrodynamics in Superconducting Circuits

EMELY WIEGAND

Department of Microtechnology and Nanoscience (MC2)
Applied Quantum Physics Laboratory
CHALMERS UNIVERSITY OF TECHNOLOGY

Göteborg, Sweden 2019

Waveguide Quantum Electrodynamics in Superconducting Circuits
EMELY WIEGAND

Thesis for the degree of Licentiate of Engineering
ISSN 1652-0769
Technical Report MC2-416

Applied Quantum Physics Laboratory
Department of Microtechnology and Nanoscience (MC2)
Chalmers University of Technology
SE-412 96 Göteborg
Sweden
Telephone: +46 (0)31-772 1000

Printed by Chalmers Reproservice
Göteborg, Sweden 2019

Waveguide Quantum Electrodynamics in Superconducting Circuits
Thesis for the degree of Licentiate of Engineering

EMELY WIEGAND

Department of Microtechnology and Nanoscience (MC2)
Applied Quantum Physics Laboratory
Chalmers University of Technology

Abstract

In the last two decades, the field of circuit quantum electrodynamics, that studies the interaction between superconducting qubits and 1-dimensional waveguides, has been of great interest. It provides a great potential to build quantum devices, which are important for quantum computing, quantum communication and quantum information. The restriction to one dimension decreases losses and information can be transferred efficiently. Superconducting qubits are artificial atoms that consist of a non-linear Josephson element and work in the microwave regime. These superconducting qubits make on-chip tunable quantum experiments possible. In the appended paper, we investigate the spontaneous emission of an initially excited artificial atom (superconducting transmon qubit) which is capacitively coupled to a semi-infinite transmission line (atom in front of a mirror). We can choose the distance to the mirror arbitrarily so the interaction with the reflected field is delayed if the qubit is far away from the mirror and we have to take time-delay effects into account. We derive equations of motion for the transmon by circuit quantization and solve them semi-classically. In this thesis we give an introduction to circuit quantization, transmission lines and superconducting qubits. Then we discuss the methods and results of the appended paper which are based on the topics introduced.

Keywords: Quantum Optics, Circuit Quantum Electrodynamics, Waveguide Quantum Electrodynamics, Superconducting Qubits, Artificial Atoms

Acknowledgements

First and foremost, I would like to express my deep gratitude to my supervisor Göran Johansson for giving me the opportunity to do my PhD in his group and for being an inspiration not only as a scientist but also as a great and supportive person. I learned a lot from him during my time at Chalmers and I am looking forward to future projects and more great discussions (may the coffee supply never run out). Special thanks go to Benjamin Rousseaux. I am very grateful to have him as a co-supervisor and friend. Without him, this work would not have been possible. Many thanks for all the valuable input and support.

More thanks go to Anton Frisk Kockum for his scientific support and supervision.

I also would like to thank all my current and former colleagues (and friends) of the Applied Quantum Physics Laboratory. I am very grateful to work in such a diverse and friendly group. I enjoy every lunch and coffee break we have together and thinking about our great discussions about different cultures, languages and what would happen if we threw Jupiter on the sun always makes me smile.

Furthermore, I would like to thank my colleagues and co-workers from Quantum Technology and Quantum Device Physics for reminding me that Physics not only happens on paper and computers. I also thank Io-Chun Hoi and everyone I met at National Tsing Hua University in Hsinchu, Taiwan for their hospitality and the valuable discussions.

Special thanks to Andreas Ask for taking the time to proof-read this thesis and giving valuable feedback.

Last but not least, I want to thank my family, friends and partner for their support.

Contents

1 Introduction

The interaction between light and matter has been of interest for more than a century. In more specific terms, the emergence of quantum mechanics has given many fundamental insights of light, its wave-particle duality, its discrete energy spectrum and its interaction with quantum systems. This has led to many of the most important inventions of the last century such as lasers and transistors. However, the devices that are commonly used work in a classical or semi-classical regime.
In the last few decades, there has been growing interest in building devices that work on a quantum level using entanglement and superpositions. Alongside of quantum computation, quantum information and quantum simulation, a new field has arisen encompassing all three of them. This new field is referred to as *Quantum Technology*. One part of quantum technology is the investigation of superconducting artificial atoms which can be used as quantum bits to build quantum computers. In the following we give an introduction to circuit quantum electrodynamics (circuit QED), where the interaction of superconducting qubits and photons is studied [1–3].

1.1 Circuit Quantum Electrodynamics

In quantum optical systems, where the interaction between light and matter, such as atoms or molecules, is studied, the coupling between the electromagnetic field and matter is rather weak since it is limited by the size of the fine structure constant [4]. In many experiments, unwanted losses to the environment exceed the coupling strength between atoms and photons, hence making information transfer difficult. To reduce the information loss, it is of advantage to engineer the environment, e.g. to restrict the system to fewer dimensions. Waveguide quantum electrodynamics (waveguide QED) studies the interaction of light and matter in one dimension [5–7], which makes it possible to reach higher coupling regimes by increasing directionality [8, 9]. It includes the investigation

of, for instance, trapped ions, Rydberg atoms in cold gases or superconducting qubits in transmission lines is studied [10]. In this work we will focus on the latter, a new field called circuit quantum electrodynamics (circuit QED), where the interaction of superconducting qubits with one-dimensional microwave transmission lines [11–14]. These artificial atoms work in the microwave regime and consist of Josephson junctions, a non-linear element, which makes the energy spectrum anharmomic, just like the energy spectrum of real atoms [15]. With superconducting qubits it is possible to reach strong and ultra-strong coupling regimes [4, 16–19], which gives the possibility to observe interesting effects, for example the superradiant phase transition [20–22].

1.2 Organization of the thesis

This thesis is organised as follows. In chapter 2, we give an introduction to circuit quantization. More specifically, we introduce superconducting circuits and their elements - transmission lines and superconducting qubits. Then we proceed in chapter 3 by demonstrating the methods and results of the appended paper, where the spontaneous emission of a superconducting artificial atom in a semi-infinite transmission line is studied. Finally, in chapter 4, we summarize the thesis and give an outlook on further research.

2 Circuit Quantization

In the appended paper, we investigate the spontaneous emission of an artificial atom connected to a one-dimensional microwave transmission line. A transmission line is a "squashed" coaxial cable that transports microwaves. It is modelled with coupled LC-oscillators. The artificial atom, that we use in the appended paper and therefore demonstrate here, is a so-called Transmon. It is a superconducting charge qubit with a transition frequency in the GHz regime. The transmon can be coupled to a transmission line, which recreates an engineerable "emitter-bath" set-up. In the following, we introduce the most important elements of superconducting circuits, such as transmission lines and superconducting qubits, and show how to quantize them [23, 24].

2.1 Lagrangian and generalised coordinates

The first step in the circuit quantization process is to define generalised coordinates ϕ_n of the system and write down the Lagrangian $\mathcal{L}$ of the circuit that contains the kinetic $\mathcal{T}$ and potential energies $\mathcal{V}$,

$$\mathcal{L}(\phi_n, \dot{\phi}_n, t) = \mathcal{T} - \mathcal{V}. \tag{2.1}$$

The kinetic energies depend on the time derivative of the generalised coordinates $\dot{\phi}_n$ and the potential energies - in a non-dispersive system - depend on the generalised coordinates ϕ_n themselves. For an electrical circuit it is convenient to use the node fluxes ϕ_n as generalised coordinates. The node fluxes are defined as the time integral of the voltage V_n at a node n,

$$\phi_n = \int_{-\infty}^{t} V_n(t)\,\mathrm{d}t. \tag{2.2}$$

In the table below we summarised some of the most important non-dispersive elements with their circuit symbols and their contribution to the energies.

Circuit Element	Symbol	Energy
Capacitor		$\mathcal{T} = \frac{1}{2}C\dot{\phi}^2$
Inductor		$\mathcal{V} = \frac{1}{2L}\phi^2$
Josephson Junction		$\mathcal{V} = E_J\left(1 - \cos\left(2\pi\frac{\phi}{\phi_0}\right)\right)$

2.2 Quantization of an LC-oscillator

We demonstrate the quantisation process of an electrical circuit by means of an LC-oscillator, depicted in Fig 2.1. The Lagrangian of this system is given by

$$\mathcal{L}(\phi, \dot{\phi}) = \frac{1}{2} C \dot{\phi}^2 - \frac{1}{2L} \phi^2, \tag{2.3}$$

with a kinetic energy term, $\mathcal{T} = \frac{1}{2} C \dot{\phi}^2$, coming from the capacitive part and the potential energy term, $\mathcal{V} = \frac{1}{2L} \phi^2$, coming from the inductive part of the circuit. The next step is to calculate the Hamiltoian $\mathcal{H}$ of the system. The Hamiltonian is a function of the node flux and its conjugate momentum, which is defined by

$$p_n = \frac{\partial \mathcal{L}}{\partial \dot{\phi}_n}, \tag{2.4}$$

and here corresponds to the node charge

$$p_n = \int_{-\infty}^{t} I_n(t) \, \mathrm{d}t, \tag{2.5}$$

where I_n is the node current. For the LC-oscillator, the conjugate momentum is given by the charge on the capacitor,

$$p = \frac{\partial \mathcal{L}}{\partial \dot{\phi}} = C \dot{\phi}. \tag{2.6}$$

In general, the Hamiltonian can be calculated by performing a change of variables using the Legendre transformation of the Lagrangian,

$$\mathcal{H}(\phi_n, p_n, t) = \sum_n p_n \dot{\phi}_n - \mathcal{L}(\phi_n, \dot{\phi}_n, t). \tag{2.7}$$

However, in the case of the LC-oscillator it is even simpler since the system is non-dispersive and holonomous-scleronomous. This means that the potential energies do not depend on the time derivative of the conjugate variable, $\partial \mathcal{V} / \partial \dot{\phi} = 0$, and the kinetic energies are quadratic in the generalised velocities $\mathcal{T}(a\dot{\phi}) = a^2 \mathcal{T}(\dot{\phi})$, where a is an arbitrary real number [25]. So the Hamiltonian is simply given by the total energy of the system

$$\mathcal{H}(\phi, q) = \mathcal{T}(p) + \mathcal{V}(\phi) = \frac{p^2}{2C} + \frac{\phi^2}{2L}. \tag{2.8}$$

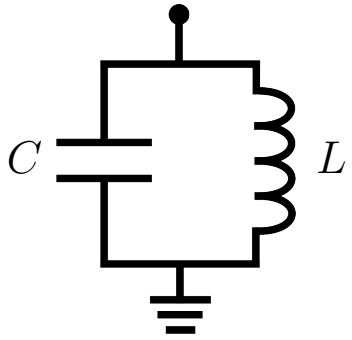

Figure 2.1: *Sketch of an LC-circuit consisting of a capacitor with capacitance C and an inductor with inductance L.*

This resembles the Hamiltonian of a harmonic oscillator $\mathcal{H} = \frac{p^2}{2m} + \frac{m}{2}\omega^2 x^2$ with frequency $\omega = 1/\sqrt{LC}$ which is the resonance frequency of the LC-oscillator and "mass" $m = C$. Now we quantise the system by promoting ϕ and p to operators

$$\phi \to \hat{\phi}, \tag{2.9}$$
$$p \to \hat{p}, \tag{2.10}$$

which fulfil the canonical commutation relation

$$\left[\hat{\phi}, \hat{p}\right] = i\hbar. \tag{2.11}$$

Now we can rewrite the Hamiltonian in terms of ladder operators a and $a^\dagger$ by defining

$$\hat{\phi} = \sqrt{\frac{\hbar}{2}\frac{1}{C\omega}}\left(a^\dagger + a\right) = \sqrt{\frac{\hbar}{2}Z}\left(a^\dagger + a\right) \tag{2.12}$$
$$\hat{p} = i\sqrt{\frac{\hbar}{2}C\omega}\left(a^\dagger - a\right) = i\sqrt{\frac{\hbar}{2Z}}\left(a^\dagger - a\right), \tag{2.13}$$

where we have introduced the characteristic impedance of the oscillator $Z = \sqrt{L/C}$.
The ladder operators a and $a^\dagger$ obey the bosonic commutation relation $\left[a, a^\dagger\right] = 1$ and operate on the energy eigenstates $|n\rangle$ in the following way

$$a|n\rangle = \sqrt{n}|n-1\rangle \tag{2.14}$$
$$a^\dagger|n\rangle = \sqrt{n+1}|n+1\rangle. \tag{2.15}$$

The rewritten Hamiltonian is given by

$$\mathcal{H} = \hbar\omega \left(a^\dagger a + \frac{1}{2} \right), \tag{2.16}$$

where $a^\dagger a = N$ is the number operator which fulfils the eigenequation $N|n\rangle = n|n\rangle$ and $\frac{\hbar\omega}{2}$ is the energy of the vacuum fluctuations.

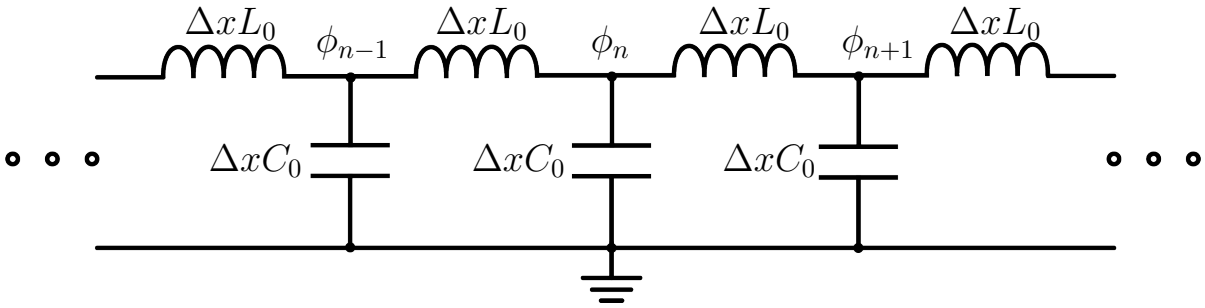

Figure 2.2: *Circuit configuration of an open transmission line. It consists of parallel grounded capacitors with capacitance C_0 per unit length Δx and inductors in series with inductance L_0 per unit length. The characteristic impedance of the transmission line is $Z_0 = \sqrt{L_0/C_0}$.*

2.3 Transmission Line

Transmission lines are one-dimensional waveguides and an important part of circuit QED, since they provide channels for the transmission of signals and they can also be used as quantum optical "baths", dissipatively removing energy from the system. They can be open systems, resonators or semi-infinite resonators with one "mirror". The differences are given by the boundary condition of the circuit configuration. We will first discuss the open transmission line and then describe possible boundary conditions.
In our system, a transmission line can be modelled with many coupled LC-oscillators, depicted in Fig 2.2 [26, 27]. The Lagrangian is given by the sum over the energies of all nodes,

$$\mathcal{L}_{TL} = \sum_n \left[\frac{1}{2} \Delta x C_0 \dot{\phi}_n^2 - \frac{1}{2} \frac{(\phi_n - \phi_{n-1})^2}{\Delta x L_0} \right]. \tag{2.17}$$

Here, the capacitances C_0 and inductances L_0 are the capacitance and inductance per unit length, since we start with a discrete circuit model. In the continuum limit $\Delta x \to \infty$, the Lagrangian becomes

$$\mathcal{L}_{TL} = \int_{-\infty}^{\infty} \left[\frac{C_0}{2} \left(\frac{\partial \phi(x,t)}{\partial t} \right)^2 + \frac{1}{2L_0} \left(\frac{\partial \phi(x,t)}{\partial x} \right)^2 \right] \mathrm{d}x. \tag{2.18}$$

Now we can calculate the Euler-Lagrange equations of motion

$$\frac{\partial}{\partial t} \frac{\partial \mathcal{L}}{\partial \frac{\partial \phi}{\partial (t,x)}} - \frac{\partial \mathcal{L}}{\partial \phi} = 0. \tag{2.19}$$

For the Lagrangian (2.18) we receive two equations which can be combined to

$$\frac{\partial \phi^2(x,t)}{\partial t^2} - c^2 \frac{\partial \phi^2(x,t)}{\partial x^2} = 0. \tag{2.20}$$

This resembles the massless Klein-Gordon equation with velocity $c = 1/\sqrt{C_0 L_0}$. Alternatively, we obtain the same equation of motion by deriving the Hamiltonian and calculating the Heisenberg equations of motion. The conjugate momenta are charges given by

$$p_n = \frac{\partial \mathcal{L}}{\partial \dot{\phi}_n} = \Delta x C_0 \dot{\phi}_n \tag{2.21}$$

so the Hamiltonian becomes

$$\mathcal{H}_{TL} = \sum_n \left[\frac{1}{2} \frac{p_n^2}{\Delta x C_0} + \frac{1}{2} \frac{(\phi_n - \phi_{n-1})^2}{\Delta x L_0} \right] \tag{2.22}$$

and in the continuum limit

$$\mathcal{H}_{TL} = \int_{-\infty}^{\infty} \left[\frac{1}{2C_0} p^2(x,t) + \frac{1}{2L_0} \left(\frac{\partial \phi(x,t)}{\partial x} \right)^2 \right] \mathrm{d}x, \tag{2.23}$$

where we introduced the flux field $\phi(x,t)$ and the charge density field $p(x,t)$. Now we quantise the system by promoting the generalised coordinates to operators which fulfil the commutation relations

$$[\phi(x,t), \phi(x',t)] = [p(x,t), p(x',t)] = 0 \tag{2.24}$$

$$[\phi(x,t), p(x',t)] = i\hbar\delta(x - x'). \tag{2.25}$$

We can solve the Klein-Gordon equation (2.20) by introducing the Fourier transform of the flux field and charge density field

$$\phi(x,t) = \frac{1}{\sqrt{2\pi}} \int_{-\infty}^{\infty} \phi(k,t) e^{ikx} \, \mathrm{d}k, \tag{2.26}$$

$$p(x,t) = \frac{1}{\sqrt{2\pi}} \int_{-\infty}^{\infty} p(k,t) e^{ikx} \, \mathrm{d}k. \tag{2.27}$$

The Klein-Gordon equation then becomes

$$\frac{\partial \phi^2(k,t)}{\partial t^2} + \omega_k^2 \phi(k,t) = 0 \tag{2.28}$$

where we used the dispersion relation $\omega_k = ck$. Now we introduce creation and annihilation operators $a_k^\dagger, a_k$, which create and annihilate a mode with wave vector k, respectively. They obey the bosonic commutation relations

$$\left[a_k, a_{k'}^\dagger\right] = \delta\left(k - k'\right), \tag{2.29}$$

$$\left[a_k, a_{k'}\right] = \left[a_k^\dagger, a_{k'}^\dagger\right] = 0, \tag{2.30}$$

and have the dimension $1/\sqrt{k}$. We rewrite the flux and charge density in terms of these operators for every mode

$$\phi(k,t) = \sqrt{\frac{\hbar}{2C_0\omega_k}}\left(a_{-k}^\dagger(t) + a_k(t)\right), \tag{2.31}$$

$$p(k,t) = i\sqrt{\frac{\hbar C_0\omega_k}{2}}\left(a_{-k}^\dagger(t) - a_k(t)\right), \tag{2.32}$$

The flux field and charge density field in real space are given by

$$\phi(x,t) = \sqrt{\frac{\hbar}{4\pi C_0}}\int_{-\infty}^{\infty}\frac{1}{\sqrt{\omega_k}}\left(a_{-k}^\dagger(t) + a_k(t)\right)e^{ikx}\,\mathrm{d}k, \tag{2.33}$$

$$p(x,t) = i\sqrt{\frac{\hbar C_0}{4\pi}}\int_{-\infty}^{\infty}\sqrt{\omega_k}\left(a_{-k}^\dagger(t) - a_k(t)\right)e^{ikx}\,\mathrm{d}k. \tag{2.34}$$

Inserting this into the Hamiltonian (2.23) we obtain

$$\mathcal{H}_{TL} = \hbar\int_{-\infty}^{\infty}\omega_k\left(a_k^\dagger a_k + \frac{1}{2}\left[a_k, a_k^\dagger\right]\right)\mathrm{d}k \tag{2.35}$$

where the commutator $\frac{1}{2}\left[a_k, a_k^\dagger\right] = \frac{1}{2}\delta(0)$ gives the (infinite) sum over the zero point energies $\hbar\omega_k/2$ of all modes [28, 29].

2.3.1 Resonator

So far we considered an open transmission line with free propagating electromagnetic waves. Now we want to restrict the propagation by considering a resonator. This can be achieved by shorting the ends of the transmission line to ground, which we demonstrate here. The circuit model and a sketch of the field of this configuration are depicted in Fig. 2.3. In this case, the field at both ends of the transmission line is zero, so the

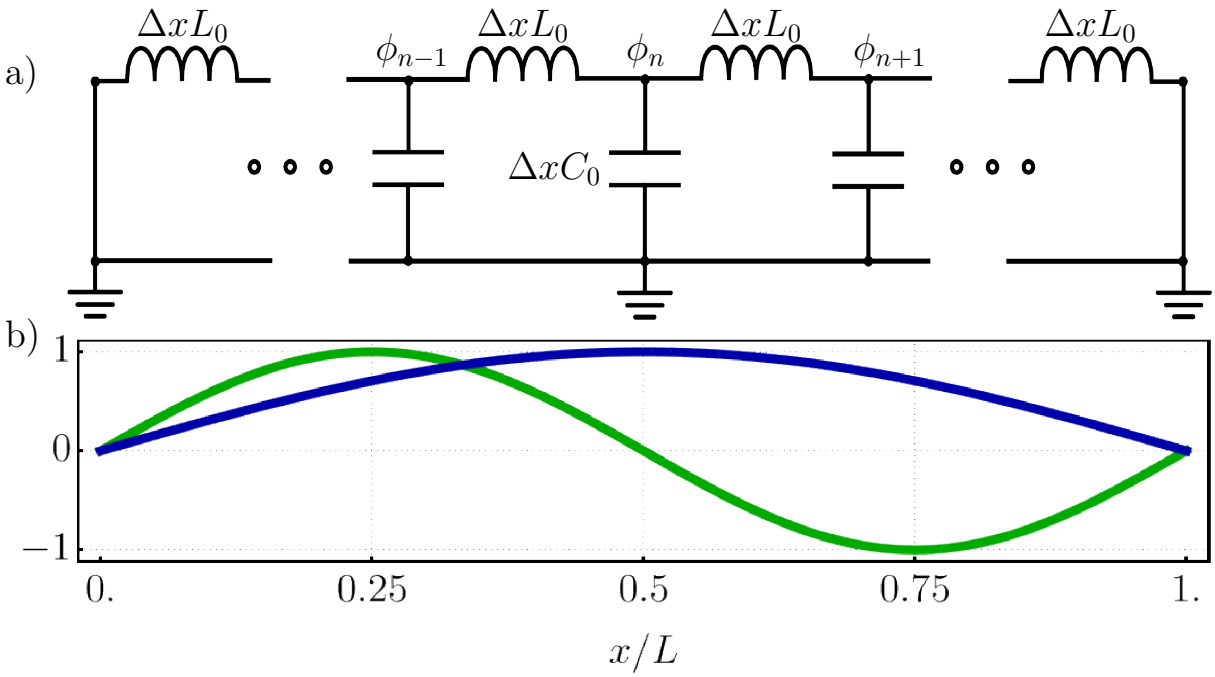

Figure 2.3: *a) Circuit model of a transmission line that is shorted to ground at both ends. By doing so the boundary conditions are restricted and the electro-magnetic field has a node at the ends. b) Two modes of the field that fulfil the boundary condition.*

field contains only modes that fulfill $\omega_n = n\pi c/L$, with $n \in \mathbb{Z}$, the length of the resonator L and the velocity of the field in the transmission line $c = 1/\sqrt{L_0 C_0}$. With this restriction, the Hamiltonian $\mathcal{H}_R$ of the resonator becomes

$$\mathcal{H}_R = \sum_n \hbar\omega_n \left(a^\dagger(\omega_n) a(\omega_n) + \frac{1}{2} \right), \tag{2.36}$$

where the operators now are dimensionless. If we only consider one mode in the field, we obtain the Hamiltonian of a single-mode quantum harmonic oscillator,

$$\mathcal{H} = \hbar\omega \left(a^\dagger a + \frac{1}{2} \right). \tag{2.37}$$

2.3.2 Semi-infinite transmission line

Now we consider the case, where the transmission line is open at one side and shorted to ground on the other. The shorted end of the semi-infinite transmission line has the role of a "mirror" where the electromagnetic field

is reflected and the value of the field is zero. The circuit model of a semi-infinite transmission line is depicted in Fig. 2.4. The modes of the field are still continuous but the massless Klein-Gordon equation (2.20) has to be solved with the boundary condition $\phi(x = x_0) = 0$, were the "mirror" is located at $x = x_0$. The solution therefore contains a sine function and is given by

$$\phi(x,t) = \sqrt{\frac{2}{\pi}} \int_0^\infty \phi(k,t) \sin k(x - x_0) \mathrm{d}k \tag{2.38}$$

$$p(x,t) = \sqrt{\frac{2}{\pi}} \int_0^\infty p(k,t) \sin k(x - x_0) \mathrm{d}k, \tag{2.39}$$

where $\phi(k,t)$ and $p(k,t)$ can again be written in terms of bosonic creation and annihilation operators, see Eq. (2.31)-(2.32). Using this, the field becomes

$$\phi(x,t) = \sqrt{\frac{\hbar}{\pi C_0}} \int_0^\infty \frac{1}{\sqrt{\omega_k}} \left(a_k^\dagger(t) + a_k(t)\right) \sin k(x - x_0) \mathrm{d}k, \tag{2.40}$$

$$p(x,t) = i\sqrt{\frac{\hbar C_0}{\pi}} \int_0^\infty \sqrt{\omega_k} \left(a_k^\dagger(t) - a_k(t)\right) \sin k(x - x_0) \mathrm{d}k. \tag{2.41}$$

In contrast to the open transmission line, the integral only goes from 0 to infinity because the right- and left-moving modes are connected by the mirror. We rewrite these expressions in terms of $\omega = ck$ and put it into the Hamiltonian

$$\mathcal{H}_{\text{Mirror}} = \int_{-\infty}^{x_0} \left[\frac{1}{2C_0} p^2(x,t) + \frac{1}{2L_0} \left(\frac{\partial \phi(x,t)}{\partial x} \right)^2 \right] \mathrm{d}x \tag{2.42}$$

$$= \int_0^\infty \hbar \omega a^\dagger(\omega) a(\omega) \, \mathrm{d}\omega. \tag{2.43}$$

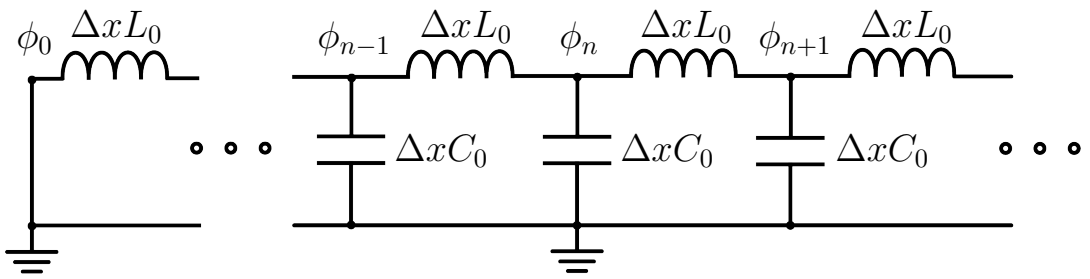

Figure 2.4: *A transmission line that is shorted to ground at one end. This end has the role of a "mirror" that reflects the electromagnetic field in the transmission line.*

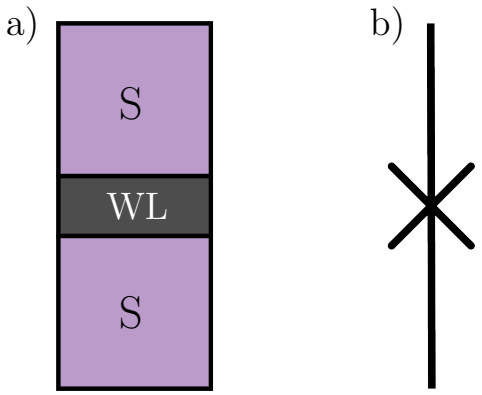

Figure 2.5: *a) A sketch of a Josephson junction. Two superconductors are separated by a weak link, where Cooper pairs can tunnel through. b) The electrical circuit symbol of a Josephson junction.*

2.4 Artificial Atoms

So far, we have investigated different set-ups of a one dimensional transmission line, that can act as different types of baths or cavities. Now we introduce emitters that can interact with the bath built of circuit elements. More specifically, we are interested in so-called artificial atoms or superconducting qubits with anharmonic energy spectrum so they can mimic real atoms and be used as qubits. There are many types of superconducting qubits with different circuit configurations and properties [13, 30]. Some examples are the flux qubit, phase qubit or the one that we are going to introduce, the transmon. The transmon is a charge qubit that consists of a Cooper pair box that is insensitive to charge noise [15]. In the following we are going to explain the basic elements of a superconducting qubit, such as the Josephson junction and the simplest version of a superconducting charge qubit, a single Cooper pair box (SCPB).

2.4.1 Josephson Junction

The Josephson junction consist of two superconductors isolated by a weak link. The weak link can consist of a thin insulator, normal metal or another superconductor [24, 31]. A sketch of a Josephson junction and the electrical circuit symbol are depicted in Fig. 2.5. The Cooper pairs can tunnel coherently through the insulator, leading to a current that varies with the phase difference across the junction,

$$I(t) = I_c \sin \varphi(t), \tag{2.44}$$

where I_c is the critical current.
The voltage across the junction is also given by the phase difference between the two superconducting leads

$$V(t) = \frac{2e}{\hbar}\frac{\partial \varphi}{\partial t}. \tag{2.45}$$

Using this, we see that the phase difference between the two superconductors φ is given by the time-integral of the voltage across the Josephson junction, which is also a magnetic flux,

$$\varphi(t) = \frac{2e}{\hbar}\int_0^t V(t')dt' = \frac{2e}{\hbar}\Phi = 2\pi\frac{\Phi}{\Phi_0}, \tag{2.46}$$

where $\Phi_0 = \frac{h}{2e}$ is the magnetic flux quantum. By comparing Eq. (2.44)-(2.45) to the general relation between the current and voltage of an inductor $\dot{I} = \frac{1}{L}V$,

$$\dot{I} = I_c \cos\varphi \frac{\partial \varphi}{\partial t} \tag{2.47}$$

$$= \frac{2\pi}{\Phi_0} I_c V \cos\varphi, \tag{2.48}$$

we find that a Josephson junction acts as a non-linear inductor with inductance

$$L_J = \frac{2\pi}{\Phi_0 I_c \cos\varphi}. \tag{2.49}$$

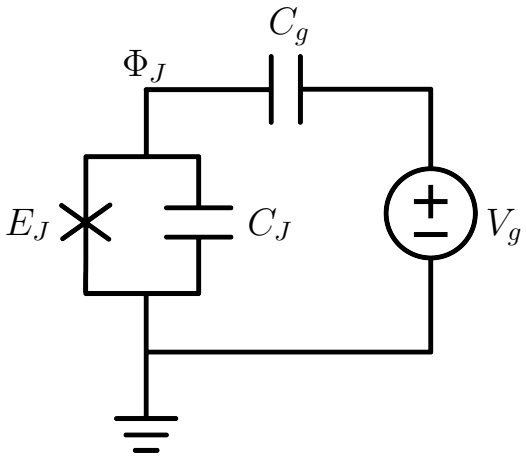

Figure 2.6: *Circuit model of a single Cooper pair box. A Josephson junction with tunnel junction capacitance C_J and Josephson coupling energy E_J is coupled to a control gate voltage V_g through a gate capacitance C_g. A number n of Cooper pair charges sit on a superconducting island ("box") between the gate capacitor and the junction capacitance.*

Now we calculate the energy that is accumulated in the Josephson junction

$$U = \int_0^t I(t)V(t)\,\mathrm{d}t \tag{2.50}$$
$$= \frac{\Phi_0}{2\pi}\int_0^t I(t)\frac{\partial\varphi}{\partial t}\,\mathrm{d}t \tag{2.51}$$
$$= \frac{\Phi_0}{2\pi}\int_0^\varphi I_c \sin\varphi\,\mathrm{d}\varphi \tag{2.52}$$
$$= E_J\,(1-\cos\varphi) \tag{2.53}$$

where we introduced the Josephson energy $E_J = \frac{\Phi_0 I_c}{2\pi}$. We see that the Josephson junction has an anharmonic potential energy which opens the possibility to build an anharmonic circuit element to create an artificial atom.
The Lagrangian of a Josephson junction is given by

$$\mathcal{L}_{\mathrm{JJ}} = \frac{1}{2}C_J\dot{\Phi} + E_J\cos\left(2\pi\frac{\Phi}{\Phi_0}\right), \tag{2.54}$$

where we neglected the constant term in the potential energy.

2.4.2 Single Cooper pair box

The single Cooper pair box (SCPB) is a simple and fundamental design for a superconducting qubit [31, 32]. It consists of a superconducting island with a number of n Cooper pair charges that is connected through

a Josephson junction to a superconducting electrode. The number of Cooper pairs can be controlled by a gate voltage that is connected to the island through a gate capacitance. A circuit model for a single Cooper pair box is depicted in Fig 2.6. The Lagrangian of the single Cooper pair box is given by

$$\mathcal{L}_{SCB} = \frac{1}{2}C_J\dot{\Phi}_J + \frac{1}{2}C_g\left(\dot{\Phi}_J + V_g\right) + E_J\cos\left(2\pi\frac{\Phi_J}{\Phi_0}\right). \tag{2.55}$$

The conjugate momentum to the node flux is given by

$$q_J = \frac{\partial\mathcal{L}}{\partial\dot{\Phi}_J} = C_J\dot{\Phi}_J + C_g\left(\dot{\Phi}_J + V_g\right) = 2en, \tag{2.56}$$

where $n = \frac{q_J}{2e}$ is the number of Cooper pairs on the island. The Hamiltonian becomes

$$\mathcal{H}_{\text{SCB}} = 4E_C\left(n - n_g\right)^2 - E_J\cos\left(2\pi\frac{\Phi_J}{\Phi_0}\right), \tag{2.57}$$

where $E_C = \frac{e^2}{2(C_g+C_J)}$ is the electron charging energy and $n_g = C_gV_g/2e$ is the (possibly fractional) number of electrons pairs that is induced on the island by the control gate. Now we quantize the Hamiltonian by promoting the number of Cooper pairs n and the node flux Φ_J to operators with commutation relation

$$\left[e^{i2\pi\frac{\hat{\Phi}_J}{\Phi_0}}, \hat{n}\right] = -e^{i2\pi\frac{\Phi_J}{\Phi_0}}. \tag{2.58}$$

In the charge basis $|n\rangle$ which are eigenstates of the number operator $\hat{n}$, $\hat{n}|n\rangle = n|n\rangle$, the Hamiltonian can be rewritten as follows [29, 31–33]

$$\mathcal{H}_{\text{SCB}} = \sum_n\left[4E_C\left(n - n_g\right)^2|n\rangle\langle n| - \frac{1}{2}E_J\left(|n+1\rangle\langle n| + |n-1\rangle\langle n|\right)\right]. \tag{2.59}$$

Having this Hamiltonian, we can calculate the energy spectrum of the single Cooper pair box. For the set-up we presented in this chapter, the charging energy E_C is usually much bigger than the Josephson energy E_J which leads to a charge-sensitive energy spectrum. We discuss this in more detail in the next section and present a charge-insensitive qubit, the Transmon.

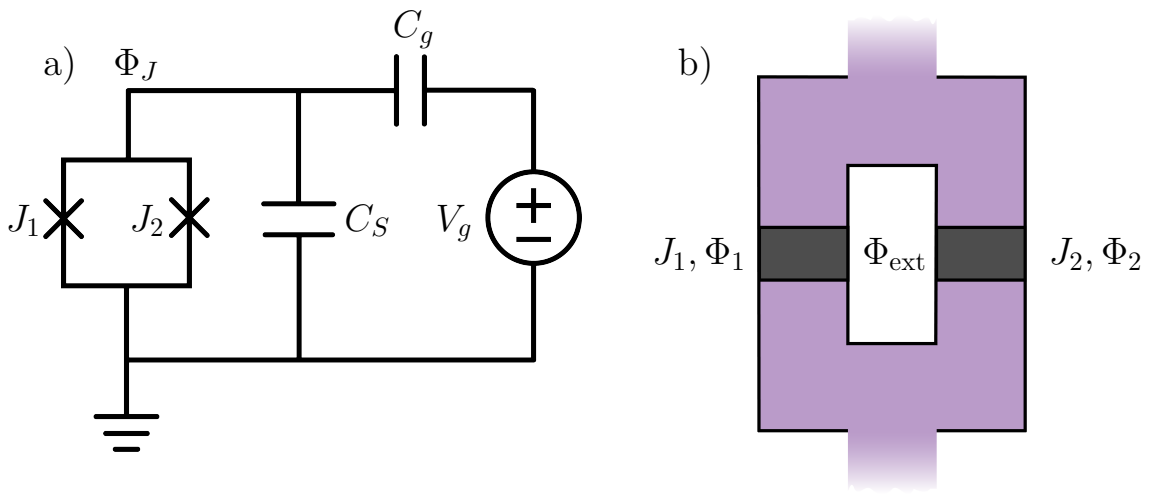

Figure 2.7: *a) Circuit model of a Transmon. A SQUID, consisting of two Josephson junctions J_1 and J_2, with an additional shunted capacitor C_S is coupled to a voltage source V_g through a gate capacitance C_g. b) Sketch of a SQUID. Two (here identical) Josephson junctions are connected in a loop. An external magnetic field induces a current in the SQUID and makes its energy controllable.*

2.4.3 The Transmon

The Transmon is a charge-insensitive superconducting qubit which was first introduced by Koch *et al.* [15] in 2007. The Transmon is a modified version of the single Cooper pair box described in the previous section. The main difference is an additional capacitance shunting the two superconductors, see Fig. 2.7 a). It is also important to mention that instead of only using one Josephson junction to create a superconducting island, the Transmon often consists of a superconducting quantum interference device (SQUID), which makes the transition frequency tunable. A sketch of a SQUID is depicted in Fig 2.7 b). By using a SQUID, the Josephson energy E_J can be manipulated through an external magnetic field, with flux Φ_{ext}, since the phases of the two Josephson junctions $\Phi_{1,2}$ depend on each other [34],

$$\Phi_1 - \Phi_2 + \Phi_{\text{ext}} = n\Phi_0, \tag{2.60}$$

where the integer number n is the number of flux quanta in the loop. The total potential energy of a SQUID (with two identical Josephson junctions) becomes

$$U = -E_{J_1} \cos\left(2\pi\frac{\Phi}{\Phi_0} + \pi\frac{\Phi_{\text{ext}}}{\Phi_0}\right) - E_{J_2} \cos\left(2\pi\frac{\Phi}{\Phi_0} - \pi\frac{\Phi_{\text{ext}}}{\Phi_0}\right) \tag{2.61}$$

$$= -E_J(\Phi_{\text{ext}}) \cos\left(2\pi \frac{\Phi}{\Phi_0}\right), \tag{2.62}$$

where $E_J(\Phi_{\text{ext}}) = 2E_{J_1} \cos\left(\pi \frac{\Phi_{\text{ext}}}{\Phi_0}\right)$ is the tunable Josephson energy. Using a SQUID instead of a single Josephson junction, thus leads to the same Hamiltonian (2.57) but with a tunable Josephson energy. However, the important element in the transmon that leads to reducing the sensitivity to charge noise, is the additional shunting capacitance, as mentioned before. With this capacitance, the charging energy $E_C = e^2/2C_\Sigma, C_\Sigma = C_J + C_g + C_S$ can be made small compared to the Josephson energy E_J. Both energies are now engineerable and the ratio E_J/E_C can be manipulated. Both the anharmonicity of the qubit and the sensitivity to charge noise depend on this ratio. In Fig 2.8 we show the energy spectrum of the Transmon as a function of the gate charge n_g. One can clearly see the reduction of sensitivity to fluctuations in gate charge by increasing the ratio E_J/E_C, since the energy levels become flat. The anharmonicity of the energy levels decreases too but it is still sufficient that the Transmon can be used as a qubit.
In the limit of small excitation amplitude $|\Phi_J/\Phi_0| \ll 0$ and $E_J \gg E_C$, where the zero point fluctuations are small, the Transmon can be approximated as a harmonic oscillator [24], where we expand the cosine term of the potential for small Φ_J,

$$\mathcal{H} = \frac{1}{2C_\Sigma} q_j^2 - E_J \cos\left(2\pi \frac{\Phi_J}{\Phi_0}\right) \tag{2.63}$$

$$\approx \frac{1}{2C_\Sigma} q_j^2 + \frac{1}{2L_J} \Phi_J^2, \tag{2.64}$$

where $L_J = \left(\frac{\hbar}{2e}\right)^2 \frac{1}{E_J}$ is the effective inductance of the oscillator. The frequency

$$\Omega_J = \frac{1}{\sqrt{C_\Sigma L_J}} = \frac{1}{\hbar}\sqrt{8E_J E_C} \tag{2.65}$$

is the resonance frequency of the harmonic oscillator and the transition frequency from the ground state to the first excited state of the Transmon.

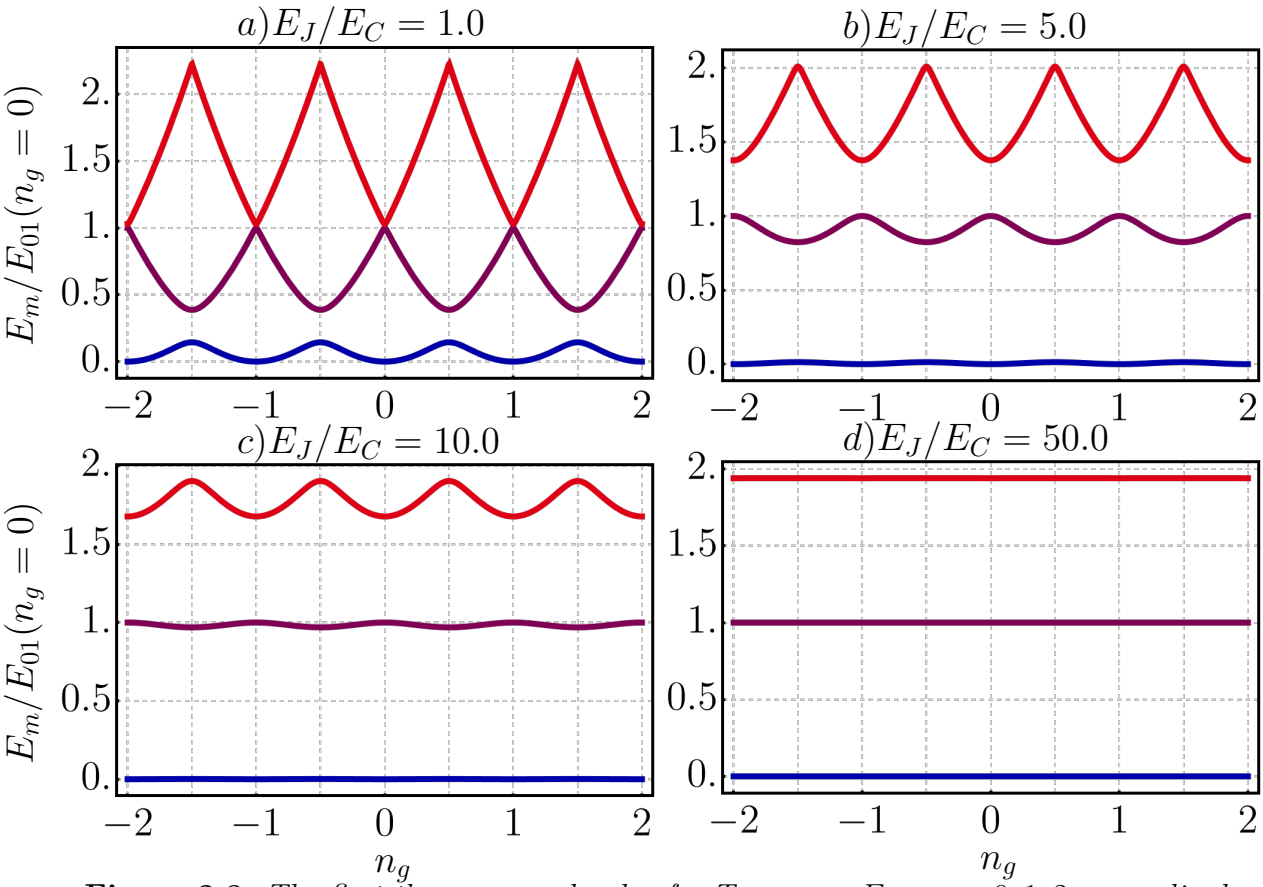

Figure 2.8: *The first three energy levels of a Transmon E_m, $m = 0, 1, 2$ normalised by the energy of the first transition E_{01} at $n_g = 0$ as a function of the charge noise n_g. The sensitivity to charge noise clearly decreases by increasing E_J/E_C.*

3 Atom in front of a mirror

In chapter 2 we introduced the quantization of electrical circuits. We discussed elements of a circuit such as transmission lines with different boundary conditions which can be viewed as a "bath". We also introduced the circuit equivalent of an atom, superconducting qubits. In the following, we investigate the combination of these two elements: A superconducting transmon qubit coupled to a semi-infinite transmission line. Strictly speaking, we investigate the spontaneous emission of an initially excited transmon coupled to a semi-infinite transmission line. In quantum optics we know that the presence of a mirror can enhance or suppress the spontaneous emission rate depending on the position of the emitter by placing it at an anti-node or node of the electromagnetic field, respectively [35]. In circuit QED, there have been experiments investigating the decay rate of an artificial atom in front of a mirror. For instance, Hoi *et al.* [36] showed theoretically that the decay rate becomes zero if the qubit is located at the node and twice as big if it is located at the anti-node of the field. Experimentally, the qubit was completely hidden when located at the node so no signal could be measured by probing the qubit. However, in this work the qubit was located very close to the mirror and the time-delay that occurs from the electromagnetic travelling to the mirror and back was neglected. Here, we take the time delay into account and investigate the transient dynamics of the qubit. We start off with a circuit QED model of the system and calculate the equations of motion. We solve the equations analytically and numerically in a semi-classical regime.

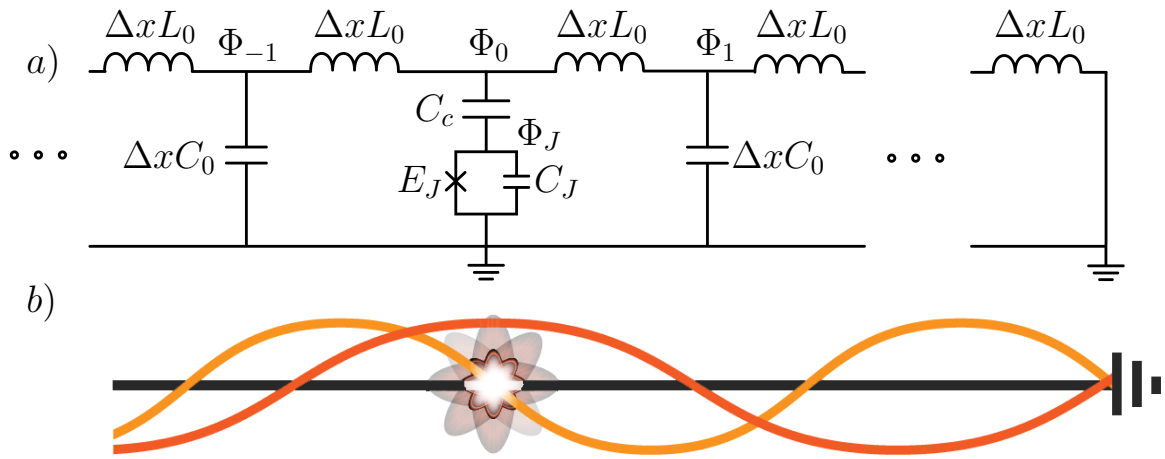

Figure 3.1: *a)Circuit model of a transmon coupled to a 1D-TL by a coupling capacitance C_c. The TL is grounded at one end. The energy, flux and capacitance of the transmon are denoted by E_J, Φ_J and C_J, respectively. The TL is modelled by LC oscillators with capacitance $\Delta x C_0$ and inductance $\Delta x L_0$. The flux of the nodes between the LC-oscillators are denoted by Φ_n. b) Sketch of the system. It depicts an atom in front of a mirror. The atom can be coupled (decoupled) to the electro-magnetic field depending on its location at the antinode (node) of an electro-magnetic mode.*

3.1 Circuit QED Model

The system we investigate consists of a transmon coupled to a 1D semi-infinite transmission line. A sketch of the system is depicted in Fig 3.1. The Hamiltonian of the system is given by the sum of all capacitive and inductive energies,

$$H(\phi_i, p_i) = \frac{1}{2C_0\Delta x}\sum_{n\neq 0} p^2_{n\neq 0}(t) + \frac{1}{2C_c}p_0^2(t) + \frac{1}{2C_J}\left(p_J(t)+p_0(t)\right)^2 + \\ + \frac{1}{2L_0\Delta x}\sum_{-\infty}^{N}\left(\phi_{n+1}(t)-\phi_n(t)\right)^2 - E_J\cos(\frac{2e}{\hbar}\phi_J(t)). \tag{3.1}$$

The Hamiltonian is a function of the generalised coordinates: ϕ_i, the node fluxes and p_i, the node charges. For details on how to derive the Hamiltonian, see the previous chapter 2. We now promote the generalised coordinates to operators that fulfil the canonical commutation relations

$$[\phi_i, p_j] = i\hbar\delta_{i,j}, \tag{3.2}$$
$$[\phi_i, \phi_j] = [p_i, p_j] = 0, \tag{3.3}$$

and calculate the Heisenberg equations of motion

$$\frac{\mathrm{d}}{\mathrm{d}t}A(t) = \frac{i}{\hbar}[H, A(t)] + \frac{\partial A(t)}{\partial t}, \tag{3.4}$$

where $A(t)$ is an arbitrary time-dependent operator. The equations of motion at the coupling point x_0, where the transmon is coupled to the TL, become

$$\partial_t \phi_0(t) = \frac{C_c + C_J}{C_c C_J} p_0(t) + \frac{1}{C_J} p_J(t), \tag{3.5}$$

$$\partial_t \phi_J(t) = \frac{1}{C_J} \left(p_J(t) + p_0(t) \right), \tag{3.6}$$

$$\partial_t p_J(t) = -E_J \frac{2e}{\hbar} \sin\left(\frac{2e}{\hbar} \phi_J(t) \right), \tag{3.7}$$

$$\partial_t p_0(t) = \frac{1}{L_0 \Delta x} \left(-2\phi_i(t) + \phi_{i+1}(t) + \phi_{i-1}(t) \right). \tag{3.8}$$

These are discrete equations of motion since they are derived by a discrete circuit model. We want to make these equations continuous by taking the limit $\Delta x \to 0$. Eq. (3.5)-(3.7) remain unchanged, but Eq. (3.8) can be rewritten as

$$\begin{aligned} \partial_t p_0(t) &= \lim_{\Delta x \to 0} \frac{1}{L_0 \Delta x} \left(-2\phi(x_0, t) + \phi(x_0 + \Delta x, t) + \phi(x_0 - \Delta x, t) \right) \\ &= \lim_{\Delta x \to 0} \frac{1}{L_0} \left(\frac{\phi(x_0 + \Delta x, t) - \phi(x_0, t)}{\Delta x} - \frac{\phi(x_0, t) - \phi(x_0 - \Delta x, t)}{\Delta x} \right) \\ &= \frac{1}{L_0} \left(\partial_x \phi(x_0^+, t) - \partial_x \phi(x_0^-, t) \right), \end{aligned} \tag{3.9}$$

where we identified the two terms of the second row as first order spatial derivatives. $\phi(x_0^+, t)$ denotes the flux field of the right side of the qubit and $\phi(x_0^-, t)$ denotes the field on the left side of the qubit.

3.1.1 Linearisation of the Qubit

One important step we take to simplify our system is the linearisation of the qubit. As we showed in section 2.4, the Transmon has an anharamonic energy spectrum. In the limit $E_J \gg E_C$, the energy spectrum is only slightly anharmonic and can be approximated by a harmonic oscillator. However, we want to treat the transmon as a qubit, where only the first two energy levels are considered. In general, one has to be careful not to drive the qubit too strongly, so that the higher energy levels are not affected. In our case, we work in the single excitation regime without

driving, where the qubit can indeed be treated as a harmonic oscillator. To linearise the qubit, we expand the potential energy up to second order:

$$\begin{aligned}\mathcal{V}(\phi_J) &= -E_J \cos\left(\frac{2e}{\hbar}\phi_J\right) \\ &= -E_J\left(1 - \frac{1}{2!}\left(\frac{2e}{\hbar}\right)^2 \phi_J^2 + \mathcal{O}\left(\left(\frac{2e}{\hbar}\right)^4 \phi_J^4\right)\right) \\ &\approx \frac{\phi_J^2}{2L_J}\end{aligned} \tag{3.10}$$

with the inductance $L_J = \frac{\hbar^2}{4e^2 E_J}$. In the last line, we neglected the constant term of the potential energy. Doing this approximation basically means, we replace the non-linear Josephson element in the circuit by an inductive element, see Fig 3.2. After the linearisation, Eq (3.7) becomes

$$\partial_t p_J(t) = -\frac{1}{L_J}\phi_J(t) \tag{3.11}$$

and we obtain a new set of differential equations for the generalised coordinates at the coupling point

$$\partial_t \phi_0(t) = \frac{C_c + C_J}{C_c C_J} p_0(t) + \frac{1}{C_J} p_J(t), \tag{3.12}$$

$$\partial_t \phi_J(t) = \frac{1}{C_J}(p_J(t) + p_0(t)), \tag{3.13}$$

$$\partial_t p_J(t) = -\frac{1}{L_J}\phi_J(t), \tag{3.14}$$

$$\partial_t p_0(t) = \frac{1}{L_0}\left(\partial_x \phi(x^+, t) - \partial_x \phi(x^-, t)\right). \tag{3.15}$$

These equations can be further reduced as we will show in the following section.

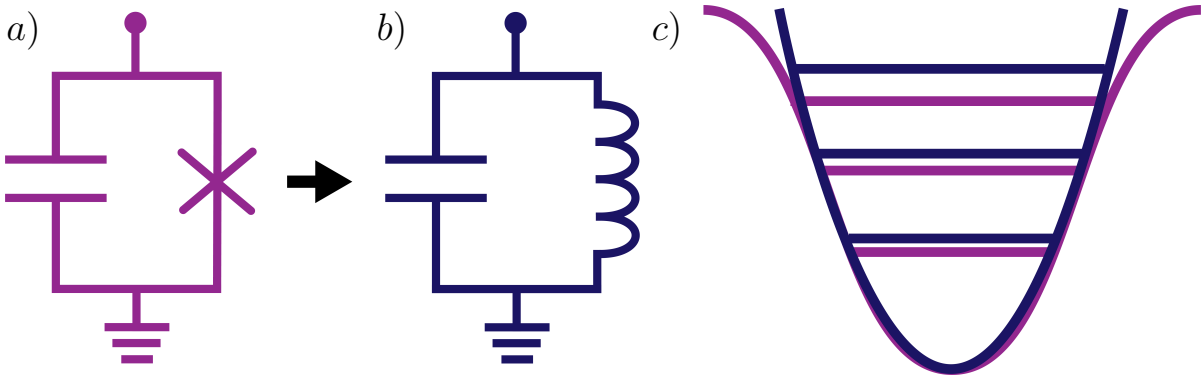

Figure 3.2: *Linearisation of the qubit means that the transmon, a), is replaced by a harmonic LC-oscillator, b). c) Anharmonic potential of the transmon and harmonic potential of the LC-oscillator. The horizontal lines denote the energy levels.*

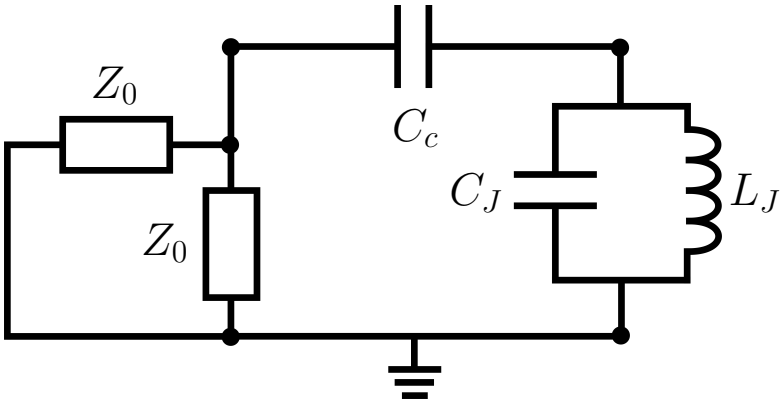

Figure 3.3: *Effective circuit model of a transmon coupled to an open TL. The transmon is replaced by an LC-oscillator with capacitance C_J and inductance L_J and is coupled to the TL via a coupling capacitance C_c. The transmission line is represented by its characteristic impedance Z_0. The photons that are emitted by the transmon can escape to both sides of the transmission line corresponding to the two parallel resistors.*

3.2 Impedance of the Transmission line

We discuss the impedance of the TL by introducing an effective circuit model, where an harmonic oscillator is coupled to an open TL which is represented by its characteristic impedance Z_0, see Fig. 3.3. The transmon is replaced by an LC-oscillator with capacitance C_J, inductance L_J and characteristic impedance $Z_J = \sqrt{L_J/C_J}$. We consider an undriven initially excited oscillator whose emitted photons can escape to both sides of the transmission line which are represented by parallel-connected resistors. In the following we want to discuss the behaviour of the system demonstrated in Fig. 3.3 by comparing the impedance of the transmission line Z_0 to the characteristic impedance of the LC-oscillator Z_J. If $Z_0/Z_J \ll 1$, the cou-

pling capacitance C_c is grounded and the system describes an undamped oscillator with resonance frequency $\omega_0 = 1/\sqrt{L_J(C_J + C_c)}$. When we on the other hand consider the opposite case $Z_0/Z_J \gg 1$, we find an undamped oscillator with resonance frequency $\omega_J = 1/\sqrt{L_J C_J}$. A common transmission line has an impedance of $Z_0 \approx 50\,\Omega$ and the impedance of a transmon is given by $Z_J \approx 2\,\mathrm{k}\Omega/\sqrt{E_J/E_C}$. The ratio E_J/E_C does usually not exceed $E_J/E_C \approx 100$, so usually we can assume that $Z_0/Z_J \leq 1$, but it has a finite value. So, in general, we have a dissipative system where energy is lost through the resistors. We are interested in the energy that is dissipated, since it gives an insight to the properties of the transmon (LC-oscillator), more specifically, its decay rate. The decay rate is defined by the energy dissipation of the LC-oscillator,

$$E(t) = E(0)e^{-\gamma t}, \tag{3.16}$$

where $E(0)$ is the initial energy of the LC oscillator. Through analysis of the circuit we find that the decay rate for $Z_0 \leq Z_J$ is given by

$$\gamma = \frac{Z_0\omega_0^2}{2}\frac{C_c^2}{C_c + C_J}. \tag{3.17}$$

For a detailed analysis, see the appended paper. In the following, we focus on the case $Z_0/Z_J \leq 1$ if not mentioned otherwise.

3.3 Field inside the transmission line

Now we take a closer look at the field inside the transmission line. The presence of the mirror creates a boundary condition and the field can not propagate freely. We want to get a close insight how the presence of the mirror affects the dynamics of the qubit. Therefore, we derive the equations of motion for the field and formulate boundary conditions. With these we are able to reduce the four equations (3.12)-(3.15) to only two equations.
The Heisenberg equations of motion of the transmission line part of the Hamiltonian are given by

$$\partial_t \phi_n(t) = \frac{1}{C_0 \Delta x} p_n(t), \tag{3.18}$$

$$\partial_t p_n(t) = \frac{1}{L_0 \Delta x} \left(-2\phi_n(t) + \phi_{n+1}(t) + \phi_{n-1}\right). \tag{3.19}$$

Again we apply the continuous limit by defining the flux field $\phi(x_n) = \phi_n(t)$ and charge density field $p(x_n, t) = p_n(t)/\Delta x$ with the spatial coordinates $x_n = n\Delta x$. In the continuum limit $\Delta x \to 0$, giving $x_n \to x$, Eq. (3.18) and (3.19) become

$$\partial_t \phi(x,t) = \frac{1}{C_0} p(x,t), \tag{3.20}$$

$$\begin{aligned} \partial_t p(x,t) &= \lim_{\Delta x \to 0} \frac{1}{L_0 \Delta x} (-2\phi(x,t) + \phi(x+\Delta x, t) + \phi(x-\Delta x, t)) \\ &= \lim_{\Delta x \to 0} \frac{1}{\Delta x L_0} \left(\frac{\phi(x+\Delta x,t) - \phi(x,t)}{\Delta x} - \frac{\phi(x,t) - \phi(x-\Delta x,t)}{\Delta x} \right) \\ &= \frac{1}{L_0} \partial_x^2 \phi(x,t), \end{aligned} \tag{3.21}$$

where we identified the terms in the second row of Eq. (3.21) as second spatial derivatives. As we already showed in section 2.3, $\phi(x,t)$ and $p(x,t)$ obey the massless Klein-Gordon equation

$$\left(\partial_t^2 - c^2 \partial_x^2\right) \phi(x,t) = 0, \tag{3.22}$$

with the velocity $c = 1/\sqrt{L_0 C_0}$ inside the transmission line. We write the solution in terms of right ($\rightarrow$) and left ($\leftarrow$) moving terms

$$\phi^{\rightleftarrows}(x,t) = \sqrt{\frac{\hbar}{4\pi C_0}} \int_0^\infty \frac{\mathrm{d}k}{\sqrt{\omega_k}} \left(a_k^{\rightleftarrows} e^{-i(\omega_k t \mp kx)} + h.c. \right), \tag{3.23}$$

where $a_k^\dagger$ and a_k are creation and annihilation operators that create or annihilate a photon with wave vector k, respectively. They fulfil the commutation relations

$$\left[a_k, a_{k'}^\dagger\right] = \delta\left(k - k'\right), \tag{3.24}$$

$$\left[a_k, a_{k'}\right] = \left[a_k^\dagger, a_{k'}^\dagger\right] = 0. \tag{3.25}$$

The solutions can be rewritten in terms of frequencies ω and we obtain

$$\phi^{\rightleftarrows}(x,t) = \sqrt{\frac{\hbar Z_0}{4\pi}} \int_0^\infty \frac{\mathrm{d}\omega}{\sqrt{\omega}} \left(a_\omega^{\rightleftarrows} e^{-i(\omega t \mp k_\omega x)} + h.c.\right), \tag{3.26}$$

where $k_\omega = \omega/c$. In order to be able to formulate boundary conditions for the field inside the semi-infinite transmission line, we calculate the voltage $V(x,t) = \partial_t \phi(x,t)$,

$$V^{\rightleftarrows}(x,t) = -i\sqrt{\frac{\hbar Z_0}{4\pi}} \int_0^\infty \mathrm{d}\omega \sqrt{\omega} \left(a_\omega^{\rightleftarrows} e^{-i(\omega t \mp k_\omega x)} - h.c.\right) \tag{3.27}$$

an similarly, the current $I(x,t) = \partial_x \phi(x)/L_0$,

$$I^{\rightleftarrows}(x,t) = -i\sqrt{\frac{\hbar}{4\pi Z_0}} \int_0^\infty \mathrm{d}\omega \sqrt{\omega} \left(a_\omega^{\rightleftarrows} e^{-i(\omega t \mp k_\omega x)} - h.c.\right). \tag{3.28}$$

We find the relation between the voltage and the current

$$I^{\rightleftarrows}(x,t) = \frac{V^{\rightleftarrows}(x,t)}{Z_0}. \tag{3.29}$$

Now we take a look at the voltage V_0 at the coupling point x_0. Since the voltage is continuous, it can be written as the sum of the ingoing V^{in} and outgoing V^{out} voltage field on the left (L) and the right (R) sides of the qubit

$$V_0(t) = V_L^{\mathrm{in}}(t) + V_L^{\mathrm{out}}(t) = V_R^{\mathrm{in}}(t) + V_R^{\mathrm{out}}(t) = \partial_t \phi_0(t), \tag{3.30}$$

where ϕ_0 is the flux field at the coupling point. In the following we investigate the connection between the field in the TL and the transmon degrees of freedom for two different cases: An open TL and a semi-infinite TL with a mirror.

3.3.1 Open transmission line

We consider an initially excited atom with no external driving. For this reason, we assume that the average incoming vacuum field to the transmon is zero. Therefore, we find from Eq. (3.30) that the outgoing fields to the left and the right are equal,

$$V_0(t) = V_L^{\text{out}}(t) = V_R^{\text{out}}(t) = \partial_t \phi_0(t). \tag{3.31}$$

Note, that we now consider average fields and solve semi-classical equations for the system. Using that the current inside the TL is conserved we find

$$I_0 = \frac{1}{Z_0}\left(V_{\text{in}} - V_{\text{out}}\right) = -\frac{1}{Z_0} V_{\text{out}} \tag{3.32}$$

$$= -\frac{1}{Z_0}\left(V_L^{\text{out}}(t) + V_R^{\text{out}}(t)\right) \tag{3.33}$$

$$= -\frac{2}{Z_0} V_R^{\text{out}}(t) \tag{3.34}$$

and finally arrive at

$$\partial_t \phi_0(t) = -\frac{Z_0}{2} \partial_t p_0(t). \tag{3.35}$$

With this relations, the equations of motion (3.12)-(3.15) can be reduced to two equations only containing the charges p_0 and p_J,

$$\frac{C_c + C_J}{C_c C_J} p_0(t) + \frac{1}{C_J} p_J(t) = -\frac{Z_0}{2} \partial_t p_0(t), \tag{3.36}$$

$$\partial_t^2 p_J(t) = -\omega_J^2 \left(p_0(t) + p_J(t)\right). \tag{3.37}$$

3.3.2 Semi-infinite transmission line

Since the mirror is located at the right side, see Fig. 3.1. the incoming field on the right side of the qubit is given by the reflected field at the mirror. Therefore, we can write it in terms of the outgoing field on the right side with a time-delay T,

$$V_R^{\text{in}}(t) = \pm V_R^{\text{out}}(t - T), \tag{3.38}$$

where the delay-time T is given by the time it takes for the field to travel to the mirror and back. The sign is determined by the type of mirror, where

the negative sign belongs to the shorted end that we consider. Now we calculate the current at the coupling point and use current conservation

$$I_0 = \frac{2}{Z_0}\left(V_{\text{in}} - V_{\text{out}}\right) \tag{3.39}$$

where $V_{\text{in}} = V_L^{\text{in}} + V_R^{\text{in}}$ is the sum of the incoming fields on the left and the right side of the qubit and $V_{\text{out}} = V_L{}^{\text{out}} + V_R{}^{\text{out}}$ is the sum of outgoing fields on the left and the right side of the qubit. In our system, there is no incoming field from the left side, since we only look at the spontaneous emission without any driving, which means that $V_L^{\text{in}} = 0$. Therefore we find from Eq. (3.30) that

$$V_L^{\text{out}}(t) = V_R^{\text{out}}(t) + V_R^{\text{in}}(t) = V_R^{\text{out}}(t) - V_R^{\text{out}}(t-T). \tag{3.40}$$

Inserting this into Eq. (3.39) and using that the current I_0 is given by the time derivative of the charge at the coupling point, we obtain

$$\begin{aligned}
\partial_t p_0 = I_0 &= \frac{1}{Z_0}\left(V_{\text{in}} - V_{\text{out}}\right) \\
&= \frac{1}{Z_0}\left(V_L^{\text{in}} + V_R^{\text{in}} - V_L^{\text{out}} - V_R^{\text{out}}\right) \\
&= \frac{1}{Z_0}\left(-V_R^{\text{out}}(t-T) - \left(V_R^{\text{out}}(t) - V_R^{\text{out}}(t-T)\right) - V_R^{\text{out}}(t)\right) \\
\partial_t p_0 &= -\frac{2}{Z_0} V_R^{\text{out}}(t).
\end{aligned} \tag{3.41}$$

We insert this into Eq. (3.30) and find

$$\partial_t \phi_0(t) = -\frac{Z_0}{2}\partial_t\left(p_0(t) - p_0(t-T)\right). \tag{3.42}$$

Similar to the open TL case, the equations of motion (3.12)-(3.15) can be rewritten as

$$\frac{C_c + C_J}{C_c C_J} p_0(t) + \frac{1}{C_J} p_J(t) = -\frac{Z_0}{2}\partial_t\left(p_0(t) - p_0(t-T)\right), \tag{3.43}$$

$$\partial_t^2 p_J(t) = -\omega_J^2\left(p_0(t) + p_J(t)\right). \tag{3.44}$$

These equations can be reduced even more by assuming that the impedance of the TL and the coupling between the qubit and the TL is small allowing us to calculate an analytical solution, which we demonstrate in the following.

3.3.3 Weak coupling

If the impedance Z_0 is small, we find that the contribution of the right-hand side of Eq. (3.43) becomes small and we can make the following ansatz for the charge $p_0(t)$

$$p_0(t) = -\frac{C_c}{C_c + C_J} p_J(t) - \delta p_0. \tag{3.45}$$

This ansatz means that the charge on the coupling capacitance is equal to the charge of the undamped LC-oscillator plus a small perturbation. Putting this ansatz into Eq. (3.44) we find

$$\partial_t^2 p_J = -\omega_0^2 p_J + \omega_J^2 \delta p_0. \tag{3.46}$$

We solve for δp_0,

$$\delta p_0(t) = -\frac{Z_0}{2} C_J \left(\frac{C_c}{C_c + C_J}\right)^2 \partial_t \left(p_J(t) - p_J(t-T)\right) \tag{3.47}$$

$$- \frac{Z_0}{2} \frac{C_c C_J}{C_c + C_J} \partial_t \left(\delta p_0(t) - \delta p_0(t-T)\right) \tag{3.48}$$

and assume that the time derivative of the perturbation is very small, $\partial_t \delta p_0 \approx 0$ and the perturbation depends only on the charge p_J. This approximation holds in the weak coupling regime and the result coincides with methods that are commonly used in quantum optics. For details, see the appended paper. Finally, we are able to reduce Eq. (3.43) and Eq. (3.43) to

$$\partial_t^2 p_J(t) = -\omega_0^2 p_J(t) - \gamma \partial_t \left(p_J(t) - p_J(t-T)\right), \tag{3.49}$$

with the coupling strength

$$\gamma = \frac{Z_0 \omega_0^2}{2} \frac{C_c^2}{C_c + C_J}. \tag{3.50}$$

Eq. (3.49) can be solved analytically by Laplace transformation,

$$\mathcal{F}(s) = \int_0^\infty f(t) e^{-st} \, \mathrm{d}t, \tag{3.51}$$

with $s \in \mathbb{C}$. The Laplace transform of Eq. (3.49) is given by

$$\begin{aligned} s^2 \tilde{p}_J(s) - s p_J(0) - p_J'(0) = &-\omega_0^2 \tilde{p_J}(s) - \gamma s \tilde{p_J}(s) \\ &+ \gamma p_J(0) + \gamma s e^{-sT} \tilde{p_J}(s) - \gamma p_J(-T), \end{aligned} \tag{3.52}$$

and by assuming that $p_J'(0) = 0$ and $p_J(-T) = 0$ we find

$$\tilde{p}_J(s) = \frac{(\gamma + s)p_J(0)}{s^2 + \gamma s\left(1 - e^{-sT}\right) + \omega_0^2}. \tag{3.53}$$

So by applying an inverse Laplace transformation we finally arrive at

$$\begin{aligned}\frac{p_J(t)}{p_J(0)} = \sum_{n=0}^{\infty} \Theta\left(t - nT\right) \frac{\gamma^n}{n!} \Bigg\{ & e^{s_+(t-nT)} \left[\frac{d^n}{ds^n}\left(\frac{\left(s + s_+\right)^n \left(s + s_+ + \gamma\right) e^{s(t-nT)}}{\left(s + s_+ - s_-\right)^{n+1}}\right)\right]_{s=0} \\ & + e^{s_-(t-nT)} \left[\frac{d^n}{ds^n}\left(\frac{\left(s + s_-\right)^n \left(s + s_- + \gamma\right) e^{s(t-nT)}}{\left(s + s_- - s_+\right)^{n+1}}\right)\right]_{s=0} \Bigg\}. \end{aligned} \tag{3.54}$$

More details of this calculation can be found in the appendix of the appended paper and we will discuss the validity of this approximation later in section 3.4.1. In this regime we found a rigorous connection of the circuit QED model and a quantum optical emitter-bath system, see the appended paper.

3.4 Energy of the Qubit

To get an insight in the spontaneous emission of the initially excited qubit (harmonic oscillator), we calculate its energy as a function of time

$$E_q = \frac{1}{2(C_J + C_c)} p_J^2 + \frac{1}{2L_J} \phi_J^2. \tag{3.55}$$

We find a solution by numerically solving Eq. (3.43) and Eq. (3.44) and using $\phi_J = -L_J \partial_t p_J$. In Fig. 3.4, we depict the energy of the qubit as a function of time for different qubit positions with respect to the mirror compared to the open TL case (orange), which shows an exponential decay. Before we focus on the two other cases, let us discuss the influence of the mirror in general. A undriven initially excited atom in a 1-D semi-infinite TL emits photons into both directions. The photons that escape to the open side do not come back and the energy is lost. The photons that escape to the side with the mirror are reflected at the mirror and come back after a delay time T to interact with the atom again. We call one of these cycles a "round-trip". The position of the atom with respect to the mirror and the wavelength of the electromagnetic field plays a crucial roll for the dynamics of the atom. If located at an anti-node (yellow), the interaction with the reflected field enhances the emission and the decay rate increases, which can be clearly seen after the first round-trip at $t/T = 1$. This effect is known as the Purcell-effect [35]. On the other hand, if the atom is positioned at a node of the electromagnetic field, the opposite happens and the spontaneous emission is suppressed and the decay rate decreases. It even decreases so far that it becomes zero in the steady state. The energy of the qubit converges to a dark state, a state with finite excitation probability for $t \to \infty$. In the following, we discuss the dynamics of the dark state in more detail.

3.4.1 Dark State

The energy of an undriven initially excited qubit converges into a dark state if it is positioned at a node of the electromagnetic field, which means that the relationship between the transition frequency of the qubit ω_0 and the delay time T is given by $\omega_0 T = 2n\pi, n \in \mathbb{N}$.The reflected light from the mirror interacts destructively with the electromagnetic field in the TL leaving no states for the qubit to emit photons in. There are no other

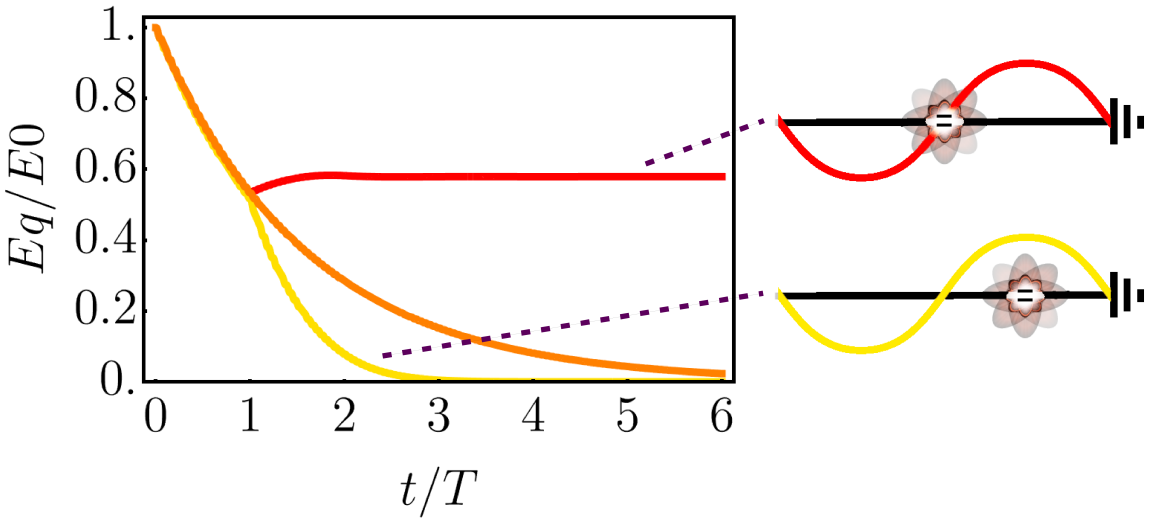

Figure 3.4: *The energy of the qubit as a function of round-trip times t/T for different positions with respect to the mirror. It shows the energy of a qubit in an open TL (orange), at a node of the field (red) and a anti-node (yellow). On the right there are sketches showing the qubit at a node and anti-node corresponding to the left figure.*

decay channels in our system so the steady state has a finite energy. We calculate the energy of the steady state by

$$\lim_{t\to\infty} f(t) = \lim_{s\to 0} s\mathcal{F}(s), \tag{3.56}$$

which we apply to Eq. (3.53). The energy of the steady state then becomes

$$\frac{E_J}{E_0} = \frac{1}{\left(1+\frac{\gamma}{2}T\right)^2}. \tag{3.57}$$

This coincides with the result of [37]. In Fig. 3.5 we depict the energy of the qubit for different values of the ratio of the coupling strength and the delay time γT. If the coupling-delay-time-ratio γT is small (green), only a small amount of energy is lost during the first round trip and the qubit reaches the dark state very quickly. For higher γT (cyan), the qubit emits all its energy during the first round-trip and the energy goes to zero. After the reflected light comes back to interact with the qubit again (at $t/T = 1$), it is re-excited and we see a revival of the energy until it reaches a steady state after several round-trip times. We note that the energy of the dark state only depends on the ratio of the coupling strength $\gamma = \frac{Z_0\omega_0^2}{2}\frac{C_c^2}{C_c+C_J}$ and the delay time T. In section 3.3.3 we made an assumption that the impedance should be small. Here, it seems that only the value of $\gamma \propto Z_0 C_c^2 \omega_0$ is important since it is proportional to the

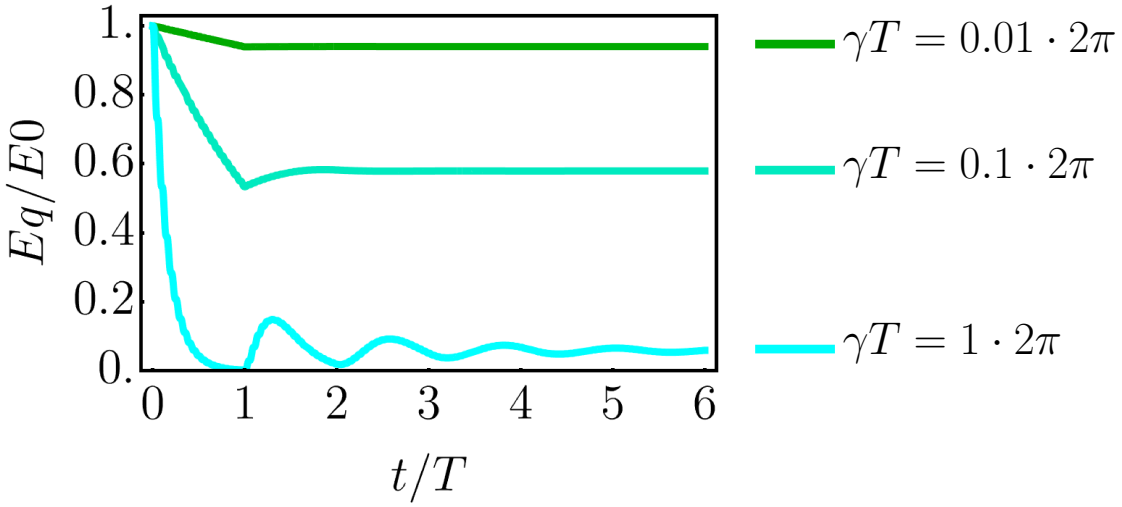

Figure 3.5: *The energy of the qubit as a function of number of round-trips t/T for different values of the coupling strength. The transient dyanamics differ a lot depending on the ratio γT. For $\gamma T = 0.01 \cdot 2\pi$ only a small amount of energy is lost during the first round-trip before the qubit reaches the dark state. For $\gamma T = 1 \cdot 2\pi$ the qubit regains energy during the first few round-trips until in converges to a dark state.*

RC-time. So the value of γ can be changed by both changing the coupling capacitance C_c or the transmission line impedance Z_0. Since we did our previous analysis with the assumption that $Z_0 \leq Z_J$, we now investigate the validity of this assumption and the approximation in section 3.3.3. In Fig. 3.6 we depict the energy of the initially excited qubit in front of a mirror for the case $Z_0 \leq Z_J$ (left) and for $Z_0 \gg Z_J$ (right), where the solid blue line corresponds to the unapproximated numerical solution and the dotted pink line corresponds to the analytical solution of Eq. (3.49), where we assumed small Z_0. In both plots the value of γ is the same. For $Z_0 \leq Z_J$ on the left, which is the case for most common transmission lines, both solutions coincide and our approximation is valid. If $Z_0 \ll Z_J$, we see that the transient dynamics differ significantly and the approximation is not valid anymore. However, both solutions converge into the same dark state, which can be easily understood by the fact that it only depends on $\gamma \propto Z_0 C_c^2 \omega_0$. So far, we only have thoroughly investigated the more common case where the TL impedance Z_0 is small. But in recent studies a new type of high-impedance transmission lines were developed, where L_0 is increases using Josephson junctions or kinetic inductances [38–40]. We leave the investigation of these open for further research.

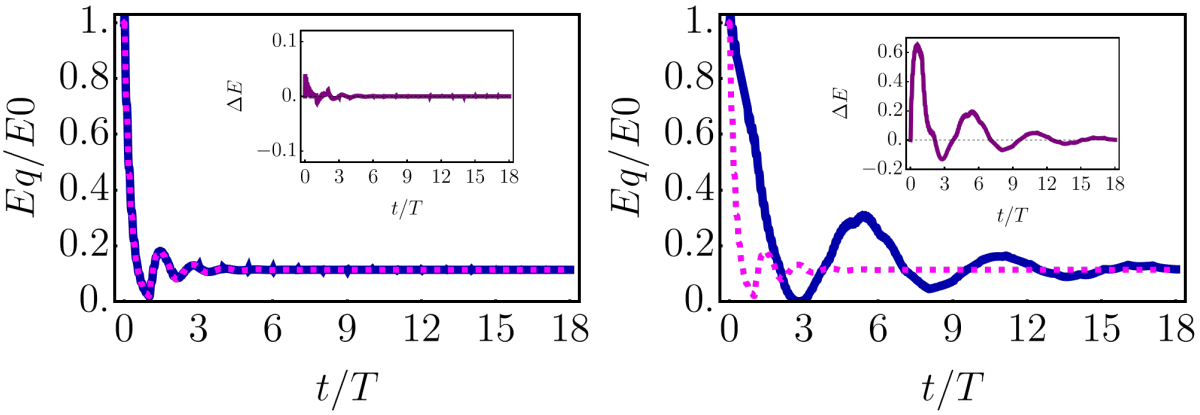

Figure 3.6: *The energy of an initially excited qubit as a function of round-trip times for the unapproximated numerical solution (solid blue line) and the approximated solution (dashed pink line). In both figures the value* $\gamma T = 1.25 \cdot 2\pi$ *but on the left the TL impedance is small,* $Z_0/Z_J = 1/\sqrt{2}$*, where our approximation is valid and on the right the TL impedance is big,* $Z_0/Z_J = 100$*, and our approximation breaks down.*

4 Conclusion

4.1 Summary

In this thesis, we first demonstrated how to quantize electrical circuits and introduced important parts of circuit QED, such as transmission lines and superconducting qubits (chapter 2). We demonstrated the transmission line with different boundary conditions: open transmission line, semi-infinite transmission line and a resonator. Then we introduced superconducting qubits: the single Cooper pair box and the transmon. After this, we studied their most important components, Josephson junctions, that are responsible for the anharmonic energy spectrum of artificial atoms. Then, in chapter 3, we proceeded to show results of paper 1, which is based on the theory we introduced before. We investigated an initially excited artificial atom in front of a mirror and semi-classically analysed its spontaneous emission. We explored the dynamics of the system for different positions of the atom with respect to the mirror and different coupling strengths. We also analysed the electrical circuit regarding its impedance. We found that if the atom is located at a node of the electromagnetic field, it converges into a dark state, a steady state with finite excitation probability. The value of the energy depends on the ratio between the coupling strength and the delay time, which is given by the distance to the mirror. In this thesis, we focused on the circuit QED part of the appended paper, where we also derived a quantum optical model of the system.

4.2 Open questions

We investigated the spontaneous emission of an artificial atom in front of a mirror in a semi-classical regime. This means, we neglected dephasing, which leads to fluctuations in the transition frequency of the qubit, so a dark state could be difficult to reach. Including dephasing in the system would be a matter of further research. Moreover, we linearised the qubit, by replacing the Josephson element in the circuit by an inductor. This leads to a harmonic energy spectrum. Since we work in the single excitation limit, we assume that this approximation is valid. However, including the non-linearity could be investigated further. Another interesting question is the investigation of high-impedance transmission lines. With our method, we are able to calculate the dynamics of an artificial atom coupled to a high-impedance transmission line, which means that we can reach strong and ultra-strong coupling regimes.

References

[1] A. González-Tudela, V. Paulisch, H. J. Kimble, and J. I. Cirac, "Efficient Multiphoton Generation in Waveguide Quantum Electrodynamics", Phys. Rev. Lett. **118**, 213601 (2017) (cit. on p. 1).

[2] V. Paulisch, H. J. Kimble, J. I. Cirac, and A. González-Tudela, "Generation of single- and two-mode multiphoton states in waveguide QED", Phys. Rev. A **97**, 053831 (2018) (cit. on p. 1).

[3] F. Quijandría, I. Strandberg, and G. Johansson, "Steady-State Generation of Wigner-Negative States in One-Dimensional Resonance Fluorescence", Phys. Rev. Lett. **121**, 263603 (2018) (cit. on p. 1).

[4] M. Devoret, S. Girvin, and R. Schoelkopf, "Circuit-QED: How strong can the coupling between a Josephson junction atom and a transmission line resonator be?", Annalen der Physik **16**, 767–779 (2007) (cit. on pp. 1, 2).

[5] H. Zheng, D. J. Gauthier, and H. U. Baranger, "Waveguide QED: Many-body bound-state effects in coherent and Fock-state scattering from a two-level system", Phys. Rev. A **82**, 063816 (2010) (cit. on p. 1).

[6] T. Tufarelli, M. S. Kim, and F. Ciccarello, "Non-Markovianity of a quantum emitter in front of a mirror", Phys. Rev. A **90**, 012113 (2014) (cit. on p. 1).

[7] E. Sanchez-Burillo, D. Zueco, J. J. Garcia-Ripoll, and L. Martin-Moreno, "Scattering in the Ultrastrong Regime: Nonlinear Optics with One Photon", Phys. Rev. Lett. **113**, 263604 (2014) (cit. on p. 1).

[8] E. Sánchez-Burillo, L. Martín-Moreno, J. J. García-Ripoll, and D. Zueco, "Full two-photon down-conversion of a single photon", Phys. Rev. A **94**, 053814 (2016) (cit. on p. 1).

[9] E. Sánchez-Burillo, D. Zueco, L. Martín-Moreno, and J. J. García-Ripoll, "Dynamical signatures of bound states in waveguide QED", Phys. Rev. A **96**, 023831 (2017) (cit. on p. 1).

[10] D. Roy, C. M. Wilson, and O. Firstenberg, "Colloquium: Strongly interacting photons in one-dimensional continuum", Rev. Mod. Phys. **89**, 021001 (2017) (cit. on p. 2).

[11] A Wallraff, D. I. Schuster, A Blais, L Frunzio, R.-S Huang, J Majer, S Kumar, S. M. Girvin, and R. J. Schoelkopf, "Strong coupling of a single photon to a superconducting qubit using circuit quantum electrodynamics", Nature **431**, 162 (2004) (cit. on p. 2).

[12] A. Blais, R. S. Huang, A. Wallraff, S. M. Girvin, and R. J. Schoelkopf, "Cavity quantum electrodynamics for superconducting electrical circuits: An architecture for quantum computation", Phys. Rev. A **69**, 1–14 (2004) (cit. on p. 2).

[13] G Wendin, "Quantum information processing with superconducting circuits: a review", Reports on Progress in Physics **80**, 106001 (2017) (cit. on pp. 2, 13).

[14] X. Gu, A. Frisk, A. Miranowicz, Y.-x. Liu, and F. Nori, "Microwave photonics with superconducting quantum circuits", Physics Reports **718-719**, 1–102 (2017) (cit. on p. 2).

[15] J. Koch, T. M. Yu, J. Gambetta, A. A. Houck, D. I. Schuster, J. Majer, A. Blais, M. H. Devoret, S. M. Girvin, and R. J. Schoelkopf, "Charge-insensitive qubit design derived from the Cooper pair box", Phys. Rev. A **76**, 1–19 (2007) (cit. on pp. 2, 13, 17).

[16] M. Bamba and T. Ogawa, "Recipe for the Hamiltonian of system-environment coupling applicable to the ultrastrong-light-matter-interaction regime", Phys. Rev. A **89**, 023817 (2014) (cit. on p. 2).

[17] A. Frisk Kockum, A. Miranowicz, S. De Liberato, S. Savasta, and F. Nori, "Ultrastrong coupling between light and matter", Nature Reviews Physics **1**, 19–40 (2019) (cit. on p. 2).

[18] D. Zueco and J. García-Ripoll, "Ultrastrongly dissipative quantum Rabi model", Phys. Rev. A **99**, 013807 (2019) (cit. on p. 2).

[19] J. A. Mlynek, A. A. Abdumalikov, C. Eichler, and A. Wallraff, "Observation of Dicke superradiance for two artificial atoms in a cavity with high decay rate", Nature Communications **5**, 5186 EP – (2014) (cit. on p. 2).

[20] P. Nataf and C. Ciuti, "No-go theorem for superradiant quantum phase transitions in cavity QED and counter-example in circuit QED", Nature Communications **1**, 72 EP – (2010) (cit. on p. 2).

[21] M. Bamba, K. Inomata, and Y. Nakamura, "Superradiant Phase Transition in a Superconducting Circuit in Thermal Equilibrium", Phys. Rev. Lett. **117**, 173601 (2016) (cit. on p. 2).

[22] M. Bamba and N. Imoto, "Circuit configurations which may or may not show superradiant phase transitions", Phys. Rev. A **96**, 053857 (2017) (cit. on p. 2).

[23] M. H. Devoret, "Quantum Fluctuations", Les Houches Session LXIII, p. 351–386 (1995) (cit. on p. 3).

[24] S. M. Girvin, *Circuit QED : Superconducting Qubits Coupled to Microwave Photons* (cit. on pp. 3, 14, 18).

[25] W. Nolting, *Grundkurs Theoretische Physik 2 - Analytische Mechanik* (Springer, 2010) (cit. on p. 5).

[26] D. M. Pozar, *Microwave Engineering* (Wiley, 2005) (cit. on p. 8).

[27] B. Yurke and J. S. Denker, "Quantum network theory", Physical Review A **29**, 1419–1437 (1984) (cit. on p. 8).

[28] M. E. Peskin and D. V. Schroeder, *An Introduction to Quantum Field Theory* (Westview Press, 1995) (cit. on p. 10).

[29] S. R. Sathyamoorthy, "Quantum Optics in Superconducting Circuits", PhD thesis (Department of Microtechnology and Nanoscience, 2017) (cit. on pp. 10, 16).

[30] J. Clarke and F. K. Wilhelm, "Superconducting quantum bits", **453**, 1031–1042 (2008) (cit. on p. 13).

[31] Y. Makhlin, G. Schön, and A. Shnirman, "Quantum-state engineering with Josephson-junction devices", Rev. Mod. Phys. **73**, 357–400 (2001) (cit. on pp. 14–16).

[32] V. Bouchiat, D. Vion, P. Joyez, D. Esteve, and M. H. Devoret, "Quantum Coherence with a Single Cooper Pair", Physica Scripta **T76**, 165 (1998) (cit. on pp. 15, 16).

[33] A. Frisk-Kockum, "Quantum Optics with Artificial Atoms", PhD thesis (Department of Microtechnology and Nanoscience, 2014) (cit. on p. 16).

[34] Y. Makhlin, G. Schön, and A. Shnirman, "Josephson-junction qubits with controlled couplings", Nature **398**, 305–307 (1999) (cit. on p. 17).

[35] E. M. Purcell, "Spontaneous emission probabilities at radio frequencies", Phys. Rev. **69**, 681 (1946) (cit. on pp. 21, 33).

[36] I. C. Hoi, A. F. Kockum, L. Tornberg, A. Pourkabirian, G. Johansson, P. Delsing, and C. M. Wilson, "Probing the quantum vacuum with an artificial atom in front of a mirror", Nature Physics **11**, 1045–1049 (2015) (cit. on p. 21).

[37] L. Guo, A. Grimsmo, A. F. Kockum, M. Pletyukhov, and G. Johansson, "Giant acoustic atom: A single quantum system with a deterministic time delay", Phys. Rev. A **95**, 053821 (2017) (cit. on p. 34).

[38] T. Weißl, B. Küng, E. Dumur, A. K. Feofanov, I. Matei, C. Naud, O. Buisson, F. W. J. Hekking, and W. Guichard, "Kerr coefficients of plasma resonances in Josephson junction chains", Phys. Rev. B **92**, 104508 (2015) (cit. on p. 35).

[39] Y. Krupko, V. D. Nguyen, T. Weißl, E. Dumur, J. Puertas, R. Dassonneville, C. Naud, F. W. J. Hekking, D. M. Basko, O. Buisson, N. Roch, and W. Hasch-Guichard, "Kerr nonlinearity in a superconducting Josephson metamaterial", Phys. Rev. B **98**, 094516 (2018) (cit. on p. 35).

[40] N. A. Masluk, I. M. Pop, A. Kamal, Z. K. Minev, and M. H. Devoret, "Microwave Characterization of Josephson Junction Arrays: Implementing a Low Loss Superinductance", Phys. Rev. Lett. **109**, 137002 (2012) (cit. on p. 35).